JACS
JOURNAL OF THE AMERICAN CHEMICAL SOCIETY

Communication

pubs.acs.org/JACS

Three-Input Logic Gates with Potential Applications for Neuronal Imaging

Kenneth S. Hettie,[‡] Jessica L. Klockow,[‡] and Timothy E. Glass*

Department of Chemistry, University of Missouri 601 South College Avenue, Columbia, Missouri 65211, United States

Supporting Information

ABSTRACT: Convenient methods for the direct visualization of neurotransmitter trafficking would bolster investigations into the development of neurodegenerative diseases. Here, tunable fluorescent molecular logic gates with applications to neuronal imaging have been developed. The three-input AND molecular logic gates are based on the coumarin-3-aldehyde scaffold and designed to give a turn-on fluorescence response upon the corelease of glutamate and zinc from secretory vesicles via exocytosis. Spectroscopic studies reveal an 11-fold fluorescence enhancement under conditions mimicking exocytosis. Methylation of the scaffold was used to optimize the spectral profile of the sensors toward desired excitation wavelengths. A binding study that elucidates the sensor-analyte interactions is presented. These sensors serve as a proof-of-concept toward the direct imaging of neurotransmitters released upon exocytosis using fluorescent molecular logic gates.

Chemical logic gates are systems where two or more semistable states possessing distinct chemical or physical properties can be reversibly interconverted.[1] Depending on the number of inputs in the system, a host of logic functions may exist which include YES, NOT, AND, OR, NOR, NAND, INHIBIT, and XOR.[2] Presently, fluorescent logic gates for bioanalytes are predominantly based on DNA, RNA, or protein underpinnings.[3,4] Biologically based fluorescent logic gates present certain drawbacks such as requiring genetic modification of the target or the risk of interference with native cell function.[3,5] On the other hand, fluorescent molecular logic gates are noninvasive, require no prior sample modification, and are compatible with cellular matrices. The literature is replete with examples of fluorescent molecular logic gates for inorganic analyte detection which function predominantly through photoinduced electron transfer processes.[1,2,6−14] However, very few fluorescent multi-input molecular logic gates have been developed for organic bioanalytes and none have been developed for organic neurotransmitters.[15]

Recently, we have developed a series of increasingly sophisticated fluorescent molecular logic gates for the direct visualization of primary amine neurotransmitters (Figure 1a).[16,17] The sensors consist of a coumarin core with functionalities integrated into the fluorophore π-system. The sensor aldehyde reversibly binds to primary amine neurotransmitters under physiological conditions to create a positively charged iminium ion which induces a large bathochromic shift in absorbance. By exciting at the new, longer wavelength, a fluorescence increase is observed due to the enhanced internal charge transfer across the π-system.

NS521 was developed as a single-input YES fluorescent molecular logic gate for the direct visualization of norepinephrine and dopamine.[16] The sensor capitalizes on the high concentrations of catecholamines (0.5−1.0 M) and acidic environment within secretory vesicles of specialized cells in order to afford selective labeling over typical cellular amines which are present at significantly lower concentrations.[16−19] We extended the utility of this method to sense neurotransmitter release by developing ES517, a dual-input AND molecular logic gate.[17] ES517 incorporates a pH-sensitive functionality into the coumarin-3-aldehyde scaffold and only fluoresces upon concomitant neurotransmitter binding and the pH change associated with exocytosis. Release of the bound complex from the acidic vesicle (pH 5) into the neutral synaptic cleft (pH 7.4) would allow for direct visualization of *only* released neurotransmitters.

A subset of glutamatergic neurons in the forebrain contain high concentrations of glutamate and zinc which are coreleased into the synaptic cleft.[21−24] These types of neurons are heavily studied, particularly with respect to the fate of the zinc ions post-exocytosis. To selectively image release from these neurons, in the presence of zinc-independent glutamatergic neurons, it would be necessary to build a sensor that not only responds to both zinc and glutamate, but also the change in pH upon exocytosis. Herein, we report a series of three-input AND fluorescent molecular logic gates that serve as a proof-of-concept for directly imaging the corelease of glutamate and zinc from glutamatergic secretory vesicles. The molecular logic gates described here are designed to exploit the copackaging of highly concentrated glutamate and zinc in glutamatergic boutons in order to directly visualize their corelease upon exocytosis. Information about glutamate and zinc corelease would offer significant insight into the mechanisms underlying neurotransmitter dysregulation and the progression of neurodegenerative diseases without altering transmission activity.[24−26]

The three-input AND gates (**1a−d**) were designed to respond to glutamate, zinc, and pH through functional groups that are integrated into the π-system of the fluorophore (Figure 1b). The aldehyde at the coumarin 3-position reversibly forms imines with glutamate and thereby, creates a multipoint binding pocket with the lactone carbonyl oxygen with which zinc can

Received: February 4, 2014
Published: March 10, 2014

   dx.doi.org/10.1021/ja501211v | *J. Am. Chem. Soc.* 2014, 136, 4877−4880

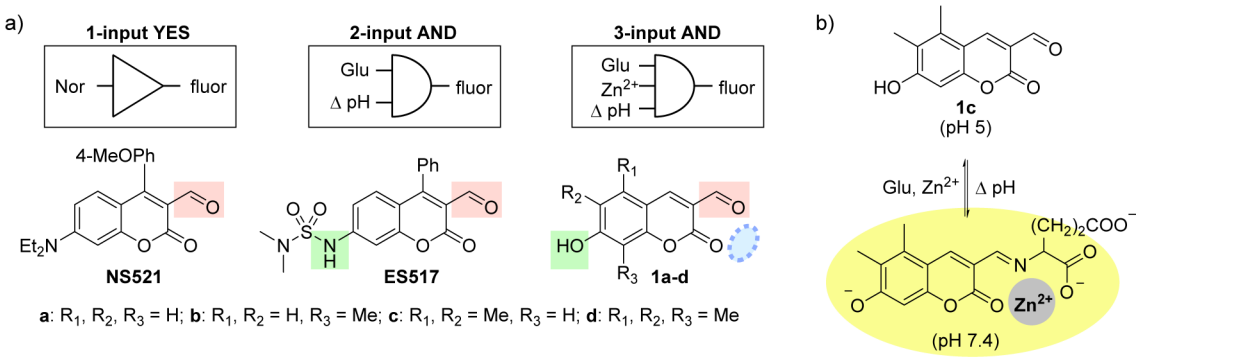

Figure 1. (a) Logic gates for neuronal imaging. (b) Binding and deprotonation of **1c**. Nor = norepinephrine, Glu = glutamate, fluor = fluorescence output, ΔpH = increase in pH from 5.0 to 7.4.

coordinate in a cooperative fashion.[27] The hydroxyl group at the 7-position imparts pH-sensitivity which acts as the final switch for a turn-on fluorescence response. Deprotonation of the hydroxyl group red-shifts the absorbance ~45 nm, permitting selective visualization of only the deprotonated species. The sensor−glutamate−zinc bound complex would be weakly fluorescent until exocytosis when the increase in pH would switch the fluorescence on. These sensors are related to NS521 and ES517, but by changing the pH-sensitive group and removing the C-4 substituent, we modify the sensor response so that fluorescence occurs only when all three inputs are present. Methyl groups were appended to the coumarin body to increase and optimize the absorption wavelengths.

The sensors were synthesized by standard methods (see Supporting Information). Titrations with glutamate and zinc were conducted and the representative spectra of sensor **1c** are shown in Figure 2. The absorbance of **1c** increases at 452 nm with the addition of glutamate; however, the fluorescence emission decreases which is opposite of the response obtained for coumarin aldehydes containing substituents at the 4-position.[16,28] Coumarin aldehydes with C-4 substituents (structure **A**) lead to a rigid iminium ion with a high quantum yield, resulting in strong fluorescence (Figure 2c).[29] However, sensor **1c** lacks a substituent at the 4-position (structure **B**) which results in free rotation of the imine and weak fluorescence.

Adding aliquots of zinc acetate to the **1c**−glutamate complex induces a hypsochromic shift in both the absorption and fluorescence maxima as well as a modest fluorescence increase (see Supporting Information). Addition of zinc rigidifies the fluorophore and locks the π-system into place, resulting in the fluorescence increase. The presence of zinc in the binding pocket prevents protonation of the imine which is otherwise protonated at physiological pH. We hypothesize that this change in protonation state mitigates the electron transfer across the fluorophore and induces the small blue shift in the spectra. A control experiment was performed in which zinc was added to sensor **1c** alone and no fluorescence change was observed.

Table 1 details the results from pH and binding titrations with sensors **1a**−**d**. Excitation and emission wavelengths increase ~10 nm with each additional methyl group, demonstrating an effective technique to tune chemosensors for specific excitation wavelengths used in conventional microscopy setups. The pK_a values of the three-input sensors were all approximately 6, which suits neuronal studies, as they will be protonated in the secretory vesicle (pH 5) and

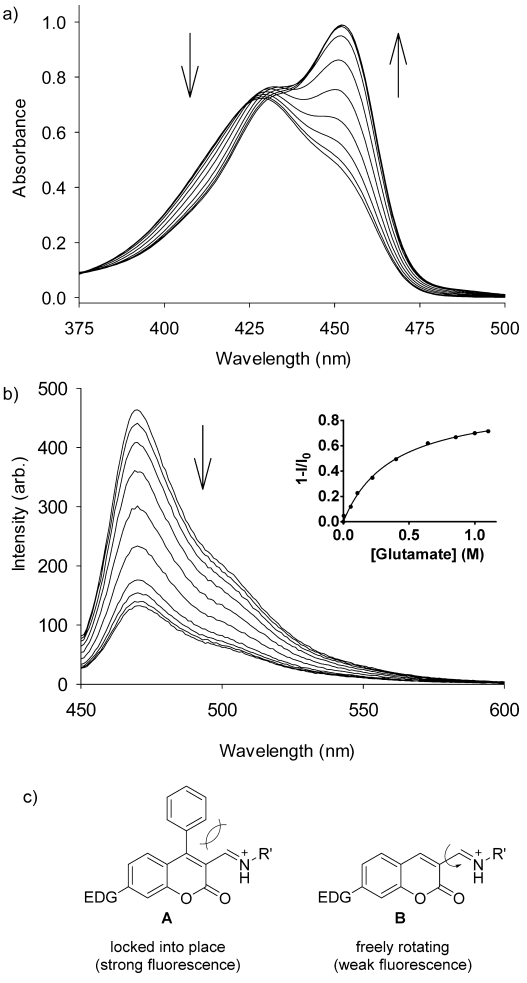

Figure 2. (a) Absorbance (20 μM) and (b) fluorescence (1 μM) titration of **1c** in buffer (50 mM bis-tris propane, 120 mM NaCl, 1% DMSO, pH 7.4) adding 20−800 μL aliquots of 1.5 M glutamate. λ_{ex} = 440 nm. Inset is the fit to a one-site binding isotherm. (c) Substituents at the coumarin 4-position inhibit free rotation of the imine. EDG = electron-donating group.

deprotonated in the synaptic cleft (pH 7.4) (see Supporting Information). Glutamate binding constants were all single-digit values, which agrees with previously obtained binding constants of coumarin aldehydes with glutamate.[16,28] The binding of zinc to the sensor−glutamate complex was comparable for all sensors and ranged from 24 to 32 M^{-1}. While these binding constants appear low, they are actually preferred for reversible

dx.doi.org/10.1021/ja501211v | J. Am. Chem. Soc. 2014, 136, 4877−4880

Table 1. Spectroscopic and Binding Properties of Sensors 1a–d

sensor	λ_{ex}, λ_{em} (nm)[a]	pK_a	K_a (Glu) (M^{-1})[b]	K_{app} (Zn^{2+}) (M^{-1})[c]	$I_{pH\ 7.4}/I_{pH\ 5.0}$[d]
1a	436, 462	6.0	2.1	24	6.7
1b	444, 472	6.1	2.6	27	9.3
1c	451, 470	6.1	2.8	30	11
1d	462, 480	5.7	2.7	32	5.8

[a]Fluorescence excitation and emission maxima of sensors **1a–d** (1 μM) in buffer (50 mM bis-tris propane, 120 mM NaCl, 1% DMSO, pH 7.4). λ_{ex} = 440 nm. [b]Binding of sensors **1a–d** (1 μM) to glutamate (Glu) in buffer (50 mM bis-tris propane, 120 mM NaCl, 1% DMSO, pH 7.4). [c]Apparent binding of sensors **1a–d** (1 μM) and glutamate (300 mM) to zinc acetate in buffer (50 mM bis-tris propane, 120 mM NaCl, 1% DMSO, pH 5.0). [d]Fluorescence intensity of a mixture of sensors **1a–d** (1 μM), glutamate (500 mM), and zinc acetate (40 mM) monitored at pH 5.0 and 7.4. λ_{ex} = 440 nm.

analyte detection because, within zinc-enriched glutamatergic secretory vesicles, glutamate and zinc are found in remarkably high concentrations (100–300 mM for glutamate and 3–30 mM for zinc).[19,20,23]

The key parameter to note is the change in fluorescence intensity ($I_{pH\ 7.4}/I_{pH\ 5.0}$) of the sensor–glutamate–zinc complex over the pH range associated with exocytosis of the vesicle. This value indicates the factor by which the fluorescence should increase upon exocytosis of the fully bound complex. The greatest fluorescence enhancement was observed with sensor **1c** at 11-fold.

The potential fluorescence outputs of sensor **1c** are shown in Figure 3. Bars a–d represent the fluorescence intensity of **1c** in

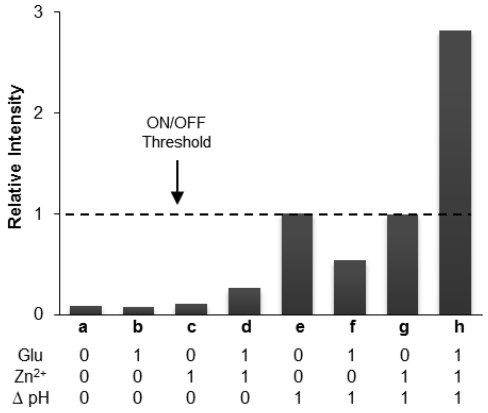

Figure 3. Relative fluorescence intensities and truth table for **1c**, a three-input AND gate. Samples contained **1c** (1 μM) in buffer (50 mM HEPES, 120 mM NaCl, 1% DMSO) in the presence or absence of glutamate (Glu, 500 mM) and zinc acetate (Zn^{2+}, 40 mM). ΔpH = increase in pH from 5.0 to 7.4.

various states *before* exocytosis (pH 5.0), and bars e–h represent the fluorescence intensity *after* exocytosis (pH 7.4). Bar h shows the only combination of inputs that gives a fluorescence turn-on response above the ON/OFF threshold using exocytotic pH conditions. Bar e depicts the next-highest fluorescence response; however, the unbound sensor is chargeless and would not accumulate within acidic secretory vesicles, but would instead be washed away during preimaging cell preparations.[16] The sensor–zinc complex (bar g) would also not be present, given the high concentration of glutamate within glutamatergic vesicles (hundreds of millimolar).[18,19] Therefore, states e and g are not even relevant to imaging applications.

To further probe the binding interaction between the sensor, the amine, and zinc, titrations were repeated with other primary amine analytes (Table 2). When added to sensor **1c**, all of the

Table 2. Spectroscopic and Binding Properties of 1c with Various Amine Analytes

Amine	K_a (amine) (M^{-1})[a]	K_{app} (Zn^{2+}) (M^{-1})[b]	$I_{pH7.4}$ / $I_{pH\ 5.0}$[c]	$I_{Glu\text{-}Zn}^{2+}$ / I_{Glu}[d]
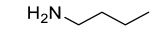 N-butylamine	0.8	-	6	0.36
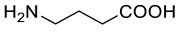 GABA	1.6	-	8	0.37
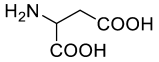 aspartic acid	1.9	24	11	1.09
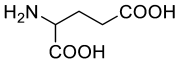 glutamic acid	2.8	30	11	2.82
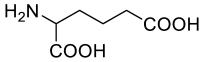 2-aminoadipic acid	2.2	26	9	2.16

[a]Binding constant of sensor **1c** (1 μM) to various amine guests in buffer (50 mM bis-tris propane, 120 mM NaCl, 1% DMSO, pH 7.4). [b]Apparent binding of **1c** (1 μM) and amine guest (300 mM) upon adding aliquots of 1.1 M zinc acetate in buffer (50 mM bis-tris propane, 120 mM NaCl, 1% DMSO, pH 5.0). [c]Fluorescence intensity of **1c** (1 μM), glutamate (500 mM), and zinc acetate (40 mM) monitored at pH 5.0 and 7.4. λ_{ex} = 440 nm. The enhancement represents the fluorescence increase upon exocytosis. [d]Ratio of the fluorescence intensity of the **1c**–amine complex with and without Zn^{2+}. λ_{ex} = 440 nm.

amines decreased the fluorescence intensity by ~65–70%, as seen with glutamate (see Supporting Information). Furthermore, there was indication that the amines containing an α-carboxylate bound better to the added zinc than did amines lacking an α-carboxylate functional group. Glutamate was still shown to have the highest fluorescence enhancement ($I_{pH\ 7.4}/I_{pH\ 5.0}$) under conditions mimicking exocytosis compared to the other analytes. We also evaluated the effect of zinc binding on the sensor–amine complex ($I_{Glu\text{-}Zn}^{2+}/I_{Glu}$). For amines containing an α-carboxylate, zinc addition increased fluorescence, but for amines lacking the α-carboxylate, zinc addition decreased fluorescence. This result also indicates that the α-carboxylate plays an important role in enabling proper zinc coordination to occur.

In conclusion, sensors **1a–d** were designed and synthesized as water-soluble three-input AND molecular logic gates for the purpose of neuronal imaging. The sensors are easily modified to incorporate multiple functionalities that are integrated into the fluorophore π-system which directly modulate the optical properties upon interaction with analyte. The unique sensing

dx.doi.org/10.1021/ja501211v | J. Am. Chem. Soc. 2014, 136, 4877–4880

mechanism capitalizes on the large quantities of glutamate already packaged in zinc-containing secretory vesicles to create a reversible binding pocket for zinc which is only visualized upon release into the synaptic cleft. The molecular logic-based approach is a proof-of-concept that may serve as a useful prototype from which other bioanalyte detection systems can be constructed.

■ ASSOCIATED CONTENT

Supporting Information

UV/vis and fluorescence spectra, synthetic procedures, and ^{1}H and ^{13}C NMR spectra. This material is available free of charge via the Internet at http://pubs.acs.org.

■ AUTHOR INFORMATION

Corresponding Author

glasst@missouri.edu

Author Contributions

‡K.S.H. and J.L.K. contributed equally.

Notes

The authors declare no competing financial interest.

■ ACKNOWLEDGMENTS

We thank the National Science Foundation (CHE-1112194) for financial support.

■ REFERENCES

(1) Sreejith, S.; Ajayaghosh, A. *Indian J. Chem. A* **2012**, *51*, 47−56.

(2) (a) de Silva, A. P. In *Molecular Logic Gates in Supramolecular Chemistry: From Molecules to Nanomaterials*; Gale, P. A., Steed, J. W., Eds.; John Wiley & Sons: Chichester, UK, 2012. (b) de Silva, A. P., *Molecular Logic-Based Computation*; Royal Society of Chemistry: London, 2012.

(3) Khalil, A. S.; Collins, J. J. *Nat. Rev. Genet.* **2010**, *11*, 367−379.

(4) Miyamoto, T.; Razavi, S.; DeRose, R.; Inoue, T. *ACS Synth. Biol.* **2013**, *2*, 72−82.

(5) Wang, B.; Kitney, R. I.; Joly, N.; Buck, M. *Nat. Commun.* **2011**, *2*, 1−9.

(6) de Silva, A. P.; Uchiyama, S. *Top. Curr. Chem.* **2011**, *300*, 1−28.

(7) de Silva, A. P.; McClenaghan, N. D. *Chem.—Eur. J.* **2004**, *10*, 574−586.

(8) Shiraishi, Y.; Tokitoh, Y.; Hirai, T. *Chem. Commun.* **2005**, 5316−5318.

(9) Magri, D. C.; Brown, G. J.; McClean, G. D.; de Silva, A. P. *J. Am. Chem. Soc.* **2006**, *128*, 4950−4951.

(10) Wang, J.; Ha, C.-S. *Sens. Actuators B-Chem.* **2010**, *146*, 373−380.

(11) Guo, X.; Zhang, D.; Zhu, D. *Adv. Mater.* **2004**, *16*, 125−130.

(12) Wang, L.; Li, B.; Zhang, L.; Luo, Y. *Dalton Trans.* **2013**, *42*, 459−465.

(13) Bozdemir, O. A.; Guliyev, R.; Buyukcakir, O.; Selcuk, S.; Kolemen, S.; Gulseren, G.; Nalbantoglu, T.; Boyaci, H.; Akkaya, E. U. *J. Am. Chem. Soc.* **2010**, *132*, 8029−8036.

(14) de Silva, A. P.; McClenaghan, N. D. *Chem.—Eur. J.* **2002**, *8*, 4935−4945.

(15) (a) Van de Bittner, G. C.; Bertozzi, C. R.; Chang, C. J. *J. Am. Chem. Soc.* **2013**, *135*, 1783−1795. (b) de Silva, A. P.; Gunaratne, H. Q. N.; McVeigh, C.; Maguire, G. E. M.; Maxwell, P. R. S.; O'Hanlon, E. *Chem. Commun.* **1996**, *18*, 2191−2192.

(16) Hettie, K. S.; Liu, X.; Gillis, K. D.; Glass, T. E. *ACS Chem. Neurosci.* **2013**, *4*, 918−923.

(17) Klockow, J. L.; Hettie, K. S.; Glass, T. E. *ACS Chem. Neurosci.* **2013**, *4*, 1334−1338.

(18) Jankowski, J. A.; Schroeder, T. J.; Ciolkowski, E. L.; Wightman, R. M. *J. Biol. Chem.* **1993**, *268*, 14694−14700.

(19) (a) Riveros, N.; Fiedler, J.; Lagos, N.; Muñoz, C.; Orrego, F. *Brain Res.* **1986**, *386*, 405−408. (b) Ottersen, O. P.; Zhang, N.; Walberg, F. *Neuroscience* **1992**, *46*, 519−534. (c) Ottersen, O. P.; Laake, J. H.; Reichelt, W.; Haug, F. M.; Torp, R. *J. Chem. Neuroanat.* **1996**, *12*, 1−14. (c) Storm-Mathisen, J.; Zhang, N.; Ottersen, O. P. *Mol. Neuropharmacol.* **1992**, *2*, 7−13. (d) Burger, P. M.; Mehl, E.; Cameron, P. L.; Maycox, P. R.; Baumert, M.; Lottspeich, F.; De Camilli, P.; Jahn, R. *Neuron* **1989**, *3*, 715−720.

(20) (a) Frederickson, C. J.; Suh, S. W.; Silva, D.; Frederickson, C. J.; Thompson, R. B. *J. Nutr.* **2000**, *130*, 1471S−83S. (b) Frederickson, C. J.; Bush, A. I. *BioMetals* **2001**, *14*, 353−366. (c) Frederickson, C. J. *Int. Rev. Neurobiol.* **1989**, *31*, 145−238.

(21) Paoletti, P.; Vergnano, A. M.; Barbour, B.; Casado, M. *Neuroscience* **2009**, *158*, 126−136.

(22) Huidobro-Toro, J. P.; Lorca, R. A.; Coddou, C. *Eur. Biophys. J.* **2008**, *37*, 301−314.

(23) Frederickson, C. J.; Hershfinkel, M.; Giblin, L. J. The Glutamatergic Synapse: Who's Talking and Who's Listening?. *Synaptic Plasticity and Transsynaptic Signaling*; Springer: New York, 2005; pp 123−137.

(24) Bitanihirwe, B. K. Y.; Cunningham, M. G. *Synapse* **2009**, *63*, 1029−1049.

(25) Sun, X.-Y.; Wei, Y.-P.; Xiong, Y.; Wang, X.-C.; Xie, A.-J.; Wang, X.-L.; Yang, Y.; Wang, Q.; Lu, Y.-M.; Wang, J.-Z.; Liu, R. *J. Biol. Chem.* **2012**, *287*, 1174−11182.

(26) Danbolt, N. C. *Prog. Neurobiol.* **2001**, *65*, 1−105.

(27) Wu, J.; Sheng, R.; Liu, W.; Wang, P.; Zhang, H.; Ma, J. *Tetrahedron* **2012**, *68*, 5458−5463.

(28) Feuster, E. K.; Glass, T. E. *J. Am. Chem. Soc.* **2003**, *125*, 16174−16175.

(29) Hettie, K. S.; Glass, T. E. **2014**, submitted.